Modeling Multi-Fraction Coastal Aeolian Sediment Transport With Horizontal and Vertical Grain-Size Variability

van IJzendoorn, C. O.; Hallin, C.; Reniers, A. J. H. M.; de Vries, S.

Important note
To cite this publication, please use the final published version (if applicable).
Please check the document version above.

JGR Earth Surface

Key Points:
- The effects of multi-fraction transport and spatial grain-size variations were examined with the numerical aeolian transport model AeoLiS
- The D_{50} can be used as a representative grain size in aeolian sediment transport modeling on a time scale of days to years
- The bed surface grain size in the upwind source area might be the most relevant to include in aeolian sediment transport models

Correspondence to:
C. O. van IJzendoorn,
c.o.vanijzendoorn@tudelft.nl

Author Contributions:
Conceptualization: C. O. van IJzendoorn, C. Hallin, A. J. H. M. Reniers, S. de Vries
Data curation: C. O. van IJzendoorn
Formal analysis: C. O. van IJzendoorn
Funding acquisition: S. de Vries
Investigation: C. O. van IJzendoorn

Modeling Multi-Fraction Coastal Aeolian Sediment Transport With Horizontal and Vertical Grain-Size Variability

C. O. van IJzendoorn[1] , **C. Hallin[1,2]**, **A. J. H. M. Reniers[1]**, and **S. de Vries[1]**

[1]Department of Hydraulic Engineering, Delft University of Technology, Delft, the Netherlands, [2]Division of Water Resources Engineering, Faculty of Engineering, Lund University, Lund, Sweden

Abstract Grain size affects the rates of aeolian sediment transport on beaches. Sediment in coastal environments typically consists of multiple grain-size fractions and exhibits spatiotemporal variations. Still, conceptual and numerical aeolian transport models are simplified and often only include a single fraction that is constant over the model domain. It is unclear to what extent this simplification is valid and if the inclusion of multi-fraction transport and spatial grain-size variations affects aeolian sediment transport simulations and predictions of coastal dune development. This study applies the numerical aeolian sediment transport model AeoLiS to compare single-fraction to multi-fraction approaches for a range of grain-size distributions and spatial grain-size scenarios. The results show that on timescales of days to years, single-fraction simulations with the median grain size, D_{50}, often give similar results to multi-fraction simulations, provided the wind is able to mobilize all fractions within that time frame. On these timescales, vertical variability in grain size has a limited effect on total transport rates, but it does influence the simulation results on minute timescales. Horizontal grain-size variability influences both the total transport rates and the downwind bed grain-size composition. The results provide new insights into the influence of beach sediment composition and spatial variability on total transport rates toward the dunes. The findings of this study can guide the implementation of grain-size variability in numerical aeolian sediment transport models.

Plain Language Summary The growth of coastal dunes is caused by the wind, which moves sand from the beach to the dunes. The sand grains on the beach have different sizes. For instance, the size of the sand grains can vary from the waterline to the start of the dunes. Small sand grains are more easily picked up by the wind than larger, heavier grains. Thus, the size of sand grains and how they are spread over the beach can impact how much sand is moved by the wind. We use computer simulations to calculate how much sand is moved by the wind under different conditions. We investigate how different assumptions about the grain size on the beach influence these calculations. The results show that the calculations with one single sand size, in most cases, give comparable results to simulations with more complicated sand size variations. The simplified approach is beneficial because it reduces the need for detailed field data of grain sizes for future calculations.

1. Introduction

Sediment available for aeolian transport in coastal settings is characterized by a grain-size distribution that is typically described with a range of grain-size fractions (Krumbein, 1934). Grain size affects aeolian sediment transport due to the larger drag and lift force that is necessary to displace coarser grains (Durán et al., 2011; Sarre, 1987). Grain size also alters the creep and saltation trajectory of sediment (e.g., Cheng et al., 2015; Zhang et al., 2021). Therefore, different grain-size fractions lead to different rates of sediment transport.

Field measurements on beaches have shown considerable spatial variations in grain size in the alongshore (Hallin, Almström, et al., 2019), cross-shore (Bauer, 1991; Çelikoğlu et al., 2006; Edwards, 2001; Sonu, 1972; Stauble & Cialone, 1997; van der Wal, 2000a; van IJzendoorn et al., 2022) and vertical dimension (van IJzendoorn et al., 2022). These horizontal and vertical grain-size variations are expected to have a complex, combined effect on aeolian sediment transport, especially since grain size and sediment transport continuously interact. However, it is unknown how the spatial grain-size variability influences the rate of aeolian transport toward the dunes.

Despite the variable transport rates for the different grain-size fractions available in beach sediment, aeolian models (e.g., Hallin, Larson, & Hanson, 2019; Hoonhout & de Vries, 2016; Roelvink & Costas, 2019; van Dijk et al., 1999) are typically simplified by using a single fraction throughout the model domain (e.g., Hallin, Huisman, et al., 2019; Hoonhout & de Vries, 2016; van der Wal, 2000b). However, some models can simulate

Methodology: C. O. van IJzendoorn, C. Hallin, S. de Vries
Project Administration: C. O. van IJzendoorn
Resources: C. Hallin, S. de Vries
Software: C. O. van IJzendoorn
Supervision: C. Hallin, S. de Vries
Visualization: C. O. van IJzendoorn
Writing – original draft: C. O. van IJzendoorn
Writing – review & editing: C. Hallin, A. J. H. M. Reniers, S. de Vries

multi-fraction transport, including the effect of sorting and the associated changes to the grain-size distribution in the bed. An example of such a model is AeoLis, a process-based aeolian sediment transport model. The model has been used for multi-fraction simulations (e.g., Hoonhout & de Vries, 2016, 2019), but the difference in transport rates compared to single-fraction simulations has not yet been fully quantified.

We hypothesize that the inclusion of multi-fraction transport and spatial grain-size variations in aeolian transport simulations has a considerable effect on the calculated sediment transport. Investigating these effects in an aeolian sediment transport model can provide new insights into the functioning of the aeolian sediment transport chain. Additionally, quantifying the effects of grain size is expected to provide important recommendations for grain size as an input parameter in future aeolian transport modeling that is used for coastal dune development predictions. This quantification can also impact the use of grain size as a design parameter in the implementation of interventions in the coastal dune system (e.g., Kroon et al., 2022).

This research investigates to what extent sorting in multi-fraction sediment transport modeling and spatial grain-size variations impact aeolian sediment transport. The important processes in the aeolian sediment transport chain are discussed in Section 2.1. The choice for a numerical model as study tool is explained in Section 2.2. The numerical implementation of different grain-size scenarios that were simulated are presented in Section 3. In Section 4, the aeolian transport rates that resulted from the different grain-size scenarios are presented. These results are discussed in Section 5 and the conclusions are drawn in Section 6.

2. Background

2.1. Modeling the Aeolian Sediment Transport Chain

Model concepts of the impact of multi-fraction transport and spatial grain-size variations require that all relevant aeolian sediment transport processes are represented in the model (Figure 1). Bed stratigraphy consists of vertical layering with varying grain-size distributions (van IJzendoorn et al., 2022). The wind forcing, the horizontal influx (upwind) and outflux (downwind) of sediment, and the sediment available at the bed surface determine the rate of deposition/erosion that occurs (de Vries, Arens, et al., 2014; Houser, 2009). High wind scenarios increase the probability of erosion; however, coarse sediment at the surface can impede the pickup of sediment when armoring occurs (Gao et al., 2016; McKenna Neuman & Bédard, 2017).

Additionally, bed roughness and the fetch effect may impact whether erosion or deposition takes place. A larger bed roughness increases the transport capacity (Bagnold, 1937b). Bed roughness can vary greatly on the beach as the bed characteristics are variable and dynamic (Bristow et al., 2022; Field & Pelletier, 2018; Owen, 1964; Sherman, 1992; van Rijn & Strypsteen, 2020). The fetch effect describes how the sediment concentration in the air column increases downwind from the start of the domain until fully developed transport is reached (Bauer & Davidson-Arnott, 2002; Delgado-Fernandez, 2010; Gillette et al., 1996). Fully developed transport occurs when there is no additional pickup of sediment and the influx and outflux at a certain location are equal. Erosion and deposition of sediment results from the difference between actual and equilibrium transport.

In case of erosion, the change in bed surface grain size will be dominated by the bed stratigraphy, especially as underlying sediment layers can be exposed and armor layers can form (Hoonhout & de Vries, 2016). In the case of deposition, the change in bed surface grain size will be dominated by the grain size of the sediment in the air column. The air column is defined as all air above the bed, and no distinction is made between transport by creep, saltation and bedform migration (contrary to approaches by e.g., Sherman et al., 2019; Uphues et al., 2022). The sediment composition in the air column is determined by processes that occur upwind of the bed surface location. The sediment in the air column was picked up from the source area during antecedent wind conditions and transported toward the bed surface location (i.e., advection). During this transport, bed interaction (i.e., the splash process) might have resulted in an exchange of sediment between the air and the bed (Anderson & Haff, 1988). This exchange can alter the grain-size distribution of the sediment in the air column depending on the sediment composition of the beach between the source area and the bed surface location (Dong et al., 2004).

2.2. Studying the Role of Grain Size in the Sediment Transport Chain

In the field, it is difficult to distinguish the effect of grain-size variability from other varying environmental conditions, such as the wind field, bedforms, and surface moisture. Field measurements are often limited to
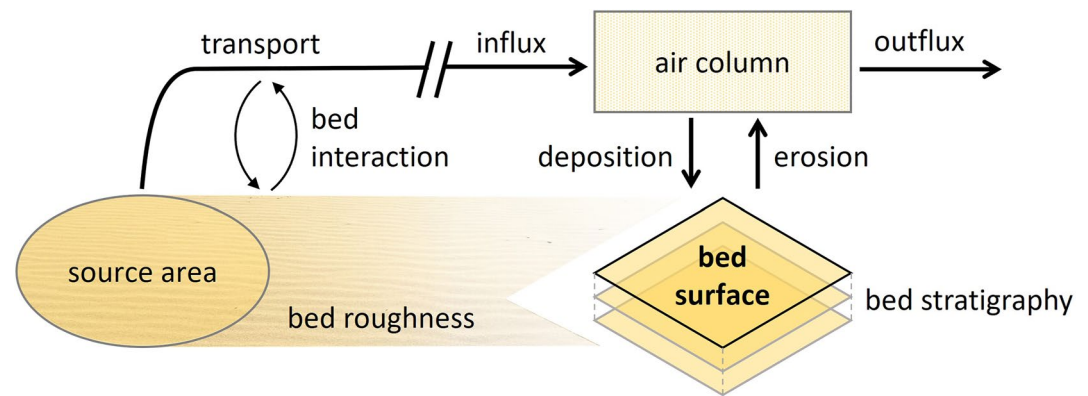
Figure 1. Conceptual representation of the interactions between sediment on the bed surface and in the air column during aeolian sediment transport on the beach that determine the grain size on the bed surface and in the air column at a specific location.

a single location, which means they can show temporal patterns in grain-size composition that are related to transport processes occurring upwind (Cohn et al., 2022; Field & Pelletier, 2018). Furthermore, it is difficult to observe the vertical bed composition at a relevant scale with non-invasive observation techniques (van IJzendoorn et al., 2022). Here, modeling has a major advantage as it allows the recording and investigation of the transport chain, including the source area, advective transport through the air, and bed surface grain size throughout the domain.

The numerical aeolian sediment transport model AeoLiS was selected as a tool to simulate the effect of grain size on aeolian transport in this research. AeoLiS provides a systematic approach to studying spatiotemporal grain-size variations. Distinguishing the impact of grain size from the many other factors that affect aeolian sediment transport on the beach is challenging. Therefore, wind tunnel experiments, in which the environmental conditions can be controlled, have been used to isolate individual aspects of aeolian sediment transport (e.g., grain size by Bagnold (1937a), and shells by McKenna Neuman et al. (2012)). However, it would be difficult if not impossible to set up experiments with complex bed composition variations at reasonable monetary, time, and labor costs. Numerical modeling provides an opportunity to gain useful insights into this type of variations at relatively low cost.

3. Methods

3.1. Model Description

The multi-fraction approach of the AeoLiS model makes it suitable to study the effect of grain-size variations on aeolian transport. The sediment bed in the model consists of a user-defined number of vertical layers and horizontal grid cells. The bed composition, which is the initial spatial grain-size variation of the bed throughout the domain, can be prescribed in the latest version of the model (AeoLiS v2.1.0 by de Vries et al., 2023). Transport, erosion and deposition are calculated for each grain-size fraction individually. Figure 2 shows how differential erosion of two different sediment fractions results in coarsening of the bed surface layer in the upwind grid cell, as fine grains are removed and coarse grains stay behind. In the downwind grid cell, the bed surface layer shows fining because the deposited sediment is a reflection of the predominantly fine sediment available in the air column. The sediment that "repletes" layer 1 in the upwind grid cell is dependent on the grain-size distribution in layer 2. The movement of excess sediment in the downwind grain cell is dependent on the original distribution in layer 1. The definition of the vertical layers is crucial for describing the process of coarsening and fining and its associated vertical grain-size gradients in the model (Hoonhout & de Vries, 2016).

In AeoLiS, the equilibrium transport rate for each individual grain-size fraction is calculated based on an adapted version of the Bagnold equation (Bagnold, 1937b), formulated as

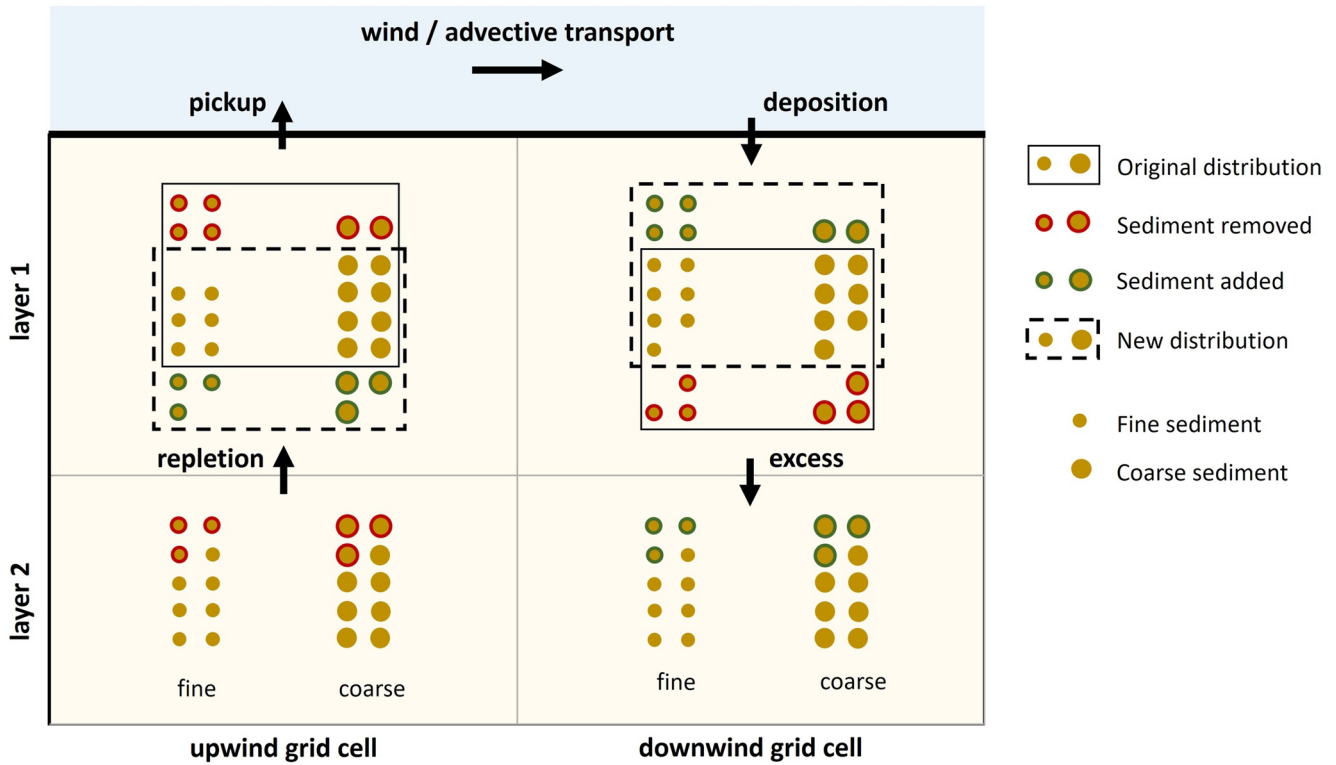$$Q = C \sqrt{\frac{d}{D}} \frac{\rho_a}{g} (u_* - u_{*,t})^3 \tag{1}$$

Figure 2. Schematization of the implementation of discrete layering in AeoLiS and the effects of erosion and deposition on the grain-size distribution. The total mass in each grid cell of each layer is normalized. This normalization is represented by the fact that each grid cell (indicated by solid and dashed, black rectangles) should contain exactly 20 sediment grains. Adapted from Hoonhout and Vries (2016).

in which Q (kg/m/s) is the aeolian sediment transport rate in the case of saturated transport, where ρ_a (kg/m³) is the density of air, and g (m/s²) is the gravitational constant. C ($-$) is a constant equal to 1.5 that accounts for sediment gradation. The value of 1.5 corresponds to a uniform sand (Bagnold, 1937b) because transport is calculated for each grain-size fraction separately. Similarly, d is the grain size of the sediment fraction for which the transport is calculated. D is a reference grain size equal to 250 μm. Following Hoonhout and de Vries (2016), $\sqrt{\frac{d}{D}}$ was initially assumed to be equal to 1. The u_* is the surface shear velocity which represents the force exerted on the surface by the wind. The $u_{*,t}$ is the threshold shear velocity which represents the shear velocity at which grains at the surface start to move (initiation of motion).

The threshold shear velocity is expressed as

$$u_{*,t} = A\sqrt{\frac{\rho_s - \rho_a}{\rho_a}g\,d} \tag{2}$$

in which ρ_s (kg/m³) is the density of the sediment, d is the grain-size diameter, and A is a dimensionless empirical constant equal to 0.085. The shear velocity is expressed as

$$u_* = u_w \frac{\kappa}{\ln\frac{z}{z_0}} \tag{3}$$

in which u_w (m/s) is the wind velocity at height z (m) and z_0 (m) is the aerodynamic roughness. The κ ($-$) represents the Von Karman constant. The z_0 depends on the surface characteristics of the bed (i.e., the bed roughness). It should be noted that, in this research, the Nikuradse roughness method (e.g., Sherman, 1992; Sherman & Farrell, 2008) was used to calculate the aerodynamic roughness ($z_0 = \frac{d}{30}$), as it allows for spatially varying grain sizes to impact the bed roughness through the median grain size, D_{50}, of the bed surface in each individual grid cell.

The equilibrium transport rate resulting from Equation 1 is used in a 1-D advection scheme (de Vries, van Thiel de Vries, et al., 2014).

$$\frac{\partial c}{\partial t} + u_z \frac{\partial c}{\partial x} = \frac{c_{\text{sat}} - c}{T} \tag{4}$$

This equation is applied to calculate the sediment mass per unit area c (kg/m^2) throughout time, indicated as t (s), and space, indicated as x (m). The u_z (m/s) represents the wind velocity at height z (m). The bed exchange, which consists of erosion and deposition, is determined as the difference between the saturated sediment concentration c_{sat} (kg/m^2) and the instantaneous sediment concentration c (i.e., the sediment concentration already present in the air) divided by an adaptation time scale T (usually 1 s). The adaptation time scale results in a simulation of the fetch effect (e.g., Bauer & Davidson-Arnott, 2002; Gillette et al., 1996), where the sediment concentration increases downwind from the start of the domain. The increase to the maximum sediment concentration (i.e., where the normalized sediment concentration equals 1) requires a longer fetch with higher wind speeds and finer grain sizes as the saturated sediment concentration increases. Additionally, the bed exchange is maximized by the sediment that is available at the bed.

For this study, the AeoLiS model was extended with the capability to input spatially varying bed grain-size properties both in the horizontal (cross-shore and longshore) and vertical domains. The source code and documentation are open-source (https://github.com/openearth/aeolis-python). More details on the model concepts in AeoLiS and their numerical implementation can be found in De Vries, van Thiel de Vries, et al. (2014) and Hoonhout and Vries (2016).

The set-up of the model used in this study was based on an idealized beach environment. The 1D domain was 200 m long with a grid size of 1 m. The seaward boundary ($x = 0$ m) had zero influx of aeolian sediment, and the landward boundary was open ($x = 200$ m), so sediment can leave the domain. In the idealized beach environment, the effect of waves and tides was excluded, and only the wind that blows over a flatbed was taken into account. The wind direction was constant and blowing in the direction of the grid from 0 to 200 m. In all simulations, nearly all default parameters of AeoLiS (v2.1.0) were used (de Vries et al., 2023). Only the parameters related to different grain-size scenarios and time scales (discussed in Sections 3.2 and 3.3), and the bed interaction parameter which determines the exchange of sediment between the air column and the bed surface (set to 0.05, following Hoonhout and Vries (2016)) deviated from the default settings.

The idealized beach environment was used to create scenarios with different temporal scales and different spatial grain-size variations. To enable the execution of the different scenarios, two main input parameters were varied: the wind forcing and the bed composition. The impact of these variations was studied by recording the sediment flux that leaves the domain. This cumulative sediment flux (in m^3/m) is a representation of the amount of sediment that is transferred from the beach to the dunes. The model setup used for all scenarios, and the python code used for the analysis and generation of the figures in this paper are freely available (van IJzendoorn, 2023).

3.2. Grain-Size Scenarios

Several grain-size scenarios were tested to investigate the effect of grain-size variability: single-fraction, multi-fraction, horizontal variation, and vertical layering. The different grain-size scenarios were simulated over different timescales with both static and variable winds to investigate the impact of sorting and wind climate. For all scenarios, a corresponding single-fraction reference grain size was used to quantify the effect of the scenario on the sediment transport. An overview of the scenarios and the 26 different cases that were formulated is presented in Table 1.

A single fraction scenario and a multi-fraction scenario, which included cases with two-fraction mixes and full particle size distributions (PSDs), were executed to investigate the effect of including multi-fraction transport in aeolian sediment transport simulations (Figure 3). For the single-fraction scenario, cases were created with one grain-size class between 125 and 2,000 μm that was the same in the entire bed (Figure 3a). In the two-fraction mix cases, grain-size classes between 125 and 2,000 μm were used. Two grain-size classes were chosen with different weights assigned to both classes for each case (Figures 3b–3d). The percentages used in the context of grain-size distributions indicate weight percentages. The single-fraction reference for 50%–50% and 80%–20% mixes was defined as the average grain size. For example, the single-fraction 375 μm case was used as the reference for the 50%–50% mix as this is the average of 250 and 500 μm. On the contrary, not the average grain size but the 125 μm case with the grain size of the most abundant fine fraction was used as a reference for the varied percentage mixes (Figure 3d).

Table 1
Overview of the Different Grain-Size Scenarios and Their Associated Cases, Including the Time Scales at Which the Cases Were Executed

Scenario	# of cases	Case description		Time scale
Single-fraction	7	125, 250, 300, 375, 500, 1,000, and 2,000 µm		10 min, 1 day, 1 year
Multi-fraction	1	Two fractions	50%–50%	1 day, <u>1 year</u>
	3		20%–80%	<u>1 day</u>, 1 year
	4		varied percentage	<u>1 day</u>, 1 year
	6	Full particle size distribution		1 day, 1 year
Spatial variations	3	Horizontal		10 min, <u>1 day</u>, 1 year
	2	Vertical		10 min, 1 day, <u>1 year</u>

Note. The underlined time scales are not shown in Section 4 because they exhibit behavior comparable to the other time scales.

For the PSD cases, 6 PSDs that resemble natural grain-size distributions were created with Qgrain (Liu et al., 2021). The shape parameters (i.e., mean, standard deviation, weight, and skewness) of the average grain-size distribution of all samples collected in Noordwijk, as presented in van IJzendoorn et al. (2022), were determined by fitting a skewed normal distribution. Subsequently, the median grain size (250 and 500 µm) and standard deviation ($\sigma = 0.32, 0.62,$ and 0.92) were varied to create 6 PSDs (Figure 3e). The single fraction cases with the median grain size of each PSD were used as the reference cases. The full PSD was expressed as the mass weight of each grain-size class with 20 classes ranging from 50 to 1,950 µm.

The effect of spatial grain-size variations on aeolian sediment transport simulations was investigated with horizontal variation and vertical layering scenarios (Figure 4). Horizontal variations were implemented with a coarse-fine, fine-coarse and fine-coarse-fine gradient (Figure 4a). To create these gradients, the weights of a fine fraction (250 µm) and a coarse fraction (500 µm) were varied between 0% and 100% along the domain. In all cases, the average distribution of the two fractions was 50%–50%; thus, the average grain size of 375 µm was used as a reference case. The different spatial distributions represent the fining and coarsening gradients found in the
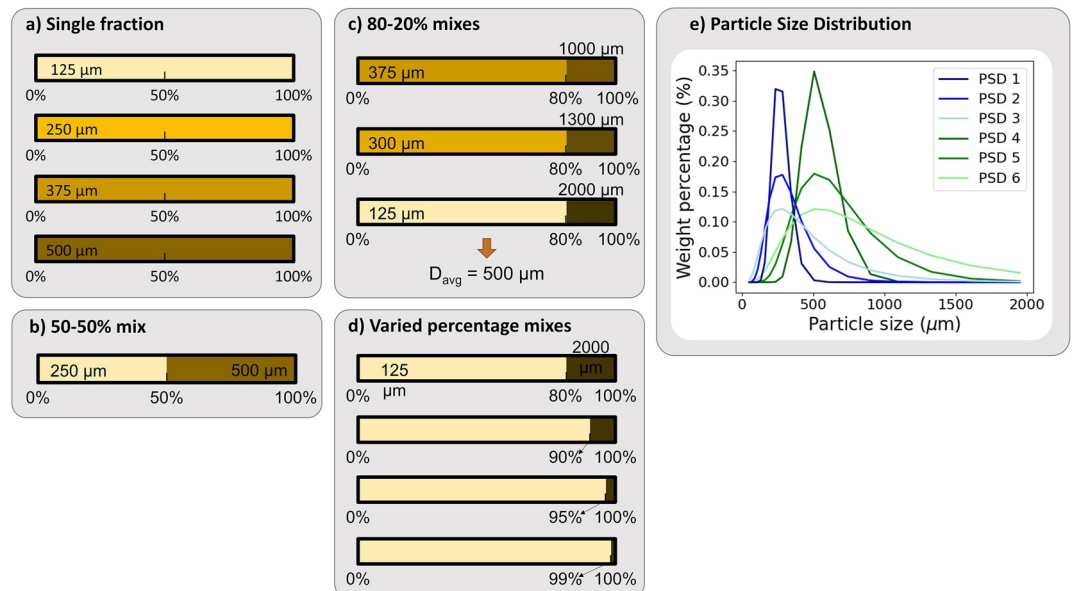

Figure 3. Overview of the different grain-size scenarios that were used in simulations with a spatially invariant grain size. For (c) the 80%–20% mixes all had the same average grain size ($D_{avg} = 500$ µm). In (d) the varied percentage mixes, two fixed grain-size classes were used (i.e., 125 and 2,000 µm), but the median grain size varied as the mass distribution over two fixed grain-size classes was varied. The (e) particle size distribution (PSD) scenario consisted of 6 different PSDs with a median grain size of approximately 250 (blue) or 500 µm (green) and varying distribution widths.
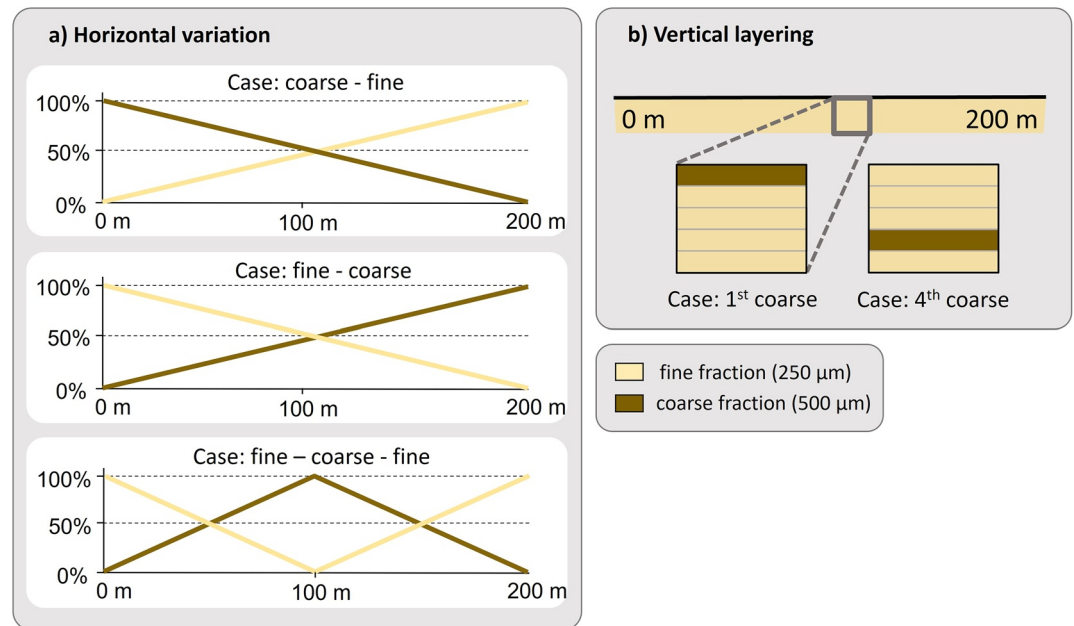
Figure 4. Overview of the different grain-size scenarios that were used in simulations with spatially varying grain-size gradients. (a) The horizontal variation scenario consisted of three different gradients where a fine (250 μm) and coarse (500 μm) grain-size class were spatially mixed. (b) In the vertical layering scenario, all layers consisted of the fine grain-size class (250 μm) apart from one coarse layer (500 μm).

field. Specifically, the gradient with coarse material in the middle represents field situations where the coarsest sediments have been found on the berm. The horizontal spatial gradients were applied to all vertical layers in the domain, including the lowest one. This results in the initial grain-size gradient being continuously supplied from below. This assumes that the initial bed stratigraphy is uniform with depth.

The effect of grain-size variations in the vertical dimension was investigated with a vertical layering scenario. In this scenario, the grain-size layering at the beach surface was represented by 5 layers, consisting of either fine (250 μm) or coarse (500 μm) sediment (Figure 4b). In the first case, the upper layer consisted of coarse sediment, whereas in the second case, the fourth layer consisted of coarse sediment. Both cases have an average grain size of 300 μm, so a single-fraction case was executed for comparison with the vertical layering scenario. In both cases, the fifth layer consisted of the same grain-size class (250 μm). This lowest layer determines the supply from below. Thus, by assigning the same grain size, large deviations between the cases were prevented that would have occurred if all superimposed sediment was eroded.

3.3. Simulation Time and Wind Forcing

Runs of 10 min, 1 day, and 1 year were executed to assess the effect of grain-size variations across time scales. The 10-min runs involved constant wind speeds between 0 and 30 m/s. The 1 day and 1 year academic cases were simulated with varying winds that were created with the wind generator in AeoLiS. The wind generator creates a random wind velocity time series with a given mean and maximum wind speed using a Markov Chain Monte Carlo approach based on a Weibull distribution. A mean wind speed of 10 m/s with a maximum wind speed of 30 m/s was used as input for the wind generator. These values were based on natural wind conditions, such as those measured by van IJzendoorn et al. (2022). Generated wind speeds fluctuate on the scale of the model time-step, dt, which was varied based on the simulation time (Table 2).

The layer thickness used in the simulations (Table 2) was scaled to the time step. This was done to avoid sediment depletion in the surface layer during time steps with peak transport, which would influence calculated transport rates. Increasing the resolution for the longer time scales is possible with a reduced time step. However, this would greatly increase the computation time needed for each simulation. We tested whether increasing the vertical resolution from 5 to 50 layers would have an effect on the 10-min time scale of the vertical layering scenario

Table 2
AeoLiS Model Settings and Wind Input for Scenarios With Different Temporal Scales

Simulation time	dt	Output_times	Wind regime	# of layers	Layer_thickness
10 min	1	10	Constant, range from 0 to 30 m/s	5	0.00005
1 day	60	600	Variable, mean 10 m/s, max 30 m/s	5	0.0001
1 year	3,600	86,400	Variable, mean 10 m/s, max 30 m/s	5	0.01

with a constant 10 m/s wind. The test showed that the cumulative sediment flux recorded at the end of the domain remained similar (i.e., a difference <3%). However, there were some minor differences in the temporal trends of the pickup of the coarse and fine sediments, which were related to (numerical) diffusion of the vertical grain-size gradient in the 5-layer test. These effects might be exacerbated at longer time scales and with the inclusion of varying wind speeds in a simulation. Therefore, the quantitative aeolian sediment transport results that were obtained at different time scales for each case were not directly compared in this paper.

4. Results

4.1. The Transport of Single-Fraction Sediment

Distinct variations in the way different grain sizes reacted to varying wind speeds on the 10 min time scale were observed in the cumulative sediment flux that was recorded at the end of the model domain (Figure 5a). Below 10 m/s, the threshold for transport was barely exceeded, and little to no sediment flux occurred for grain sizes between 250 and 500 µm (inset in Figure 5a). Between 7.5 and 12.5 m/s, the differentiation between the grain-size cases was the largest. For these wind speeds, the behavior of the shear velocity and threshold shear velocity following Equations 2 and 3 is shown in Figure 5b. As finer grain sizes have a lower threshold velocity (red line in Figure 5a), transport was initiated at lower wind speeds. For wind speeds above 12.5 m/s, sediment transport occurred in all grain-sizes. Because the shear velocity increased with the wind velocity (Equation 2) and the sediment flux is cubically related to the difference between the shear velocity and the threshold shear velocity (Equation 1), the transport that occurred at a 30 m/s wind speed was more than an order of magnitude higher than that at a 12.5 m/s wind speed.

On the 1-day time scale, a larger transport magnitude occurred for the 250 and 375 µm cases than the 500 µm case (Figure 6b). The difference in transport between the three cases was largest in the moments with high wind speeds. Throughout time, the difference in the cumulative sediment flux between the grain size cases increased
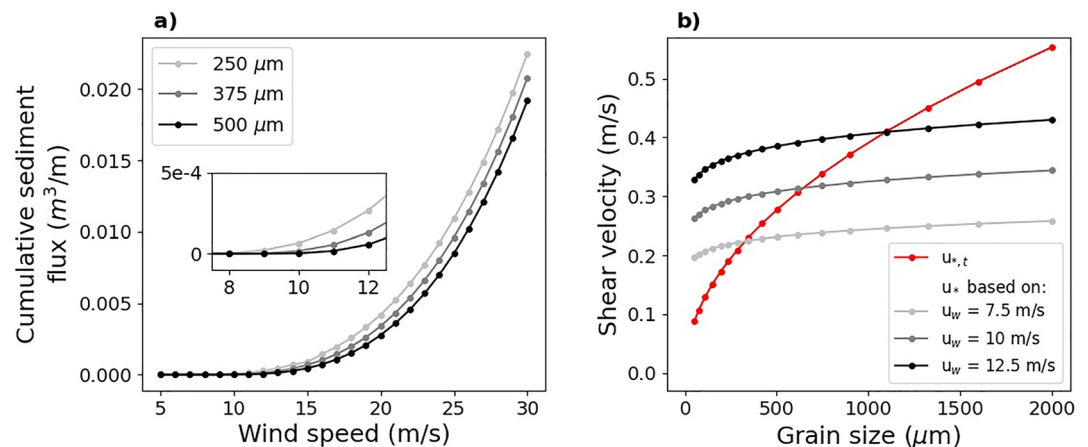

Figure 5. (a) The cumulative sediment flux after 10 min for wind speeds of 0–30 m/s for grain sizes of 250, 375, and 500 µm. The inset shows the cumulative sediment flux between wind speeds of 7.5 and 12.5 m/s. (b) The relation between grain size and the threshold shear velocity $u_{*,t}$ as follows from Equation 2 in red, and the relation between grain size and the shear velocity u_* for three different wind speeds as follows from Equation 3 (greyscale lines). The shear velocity u_* varies with grain size due to the dependence of the aerodynamic roughness z_0 on the grain size in Equation 3.
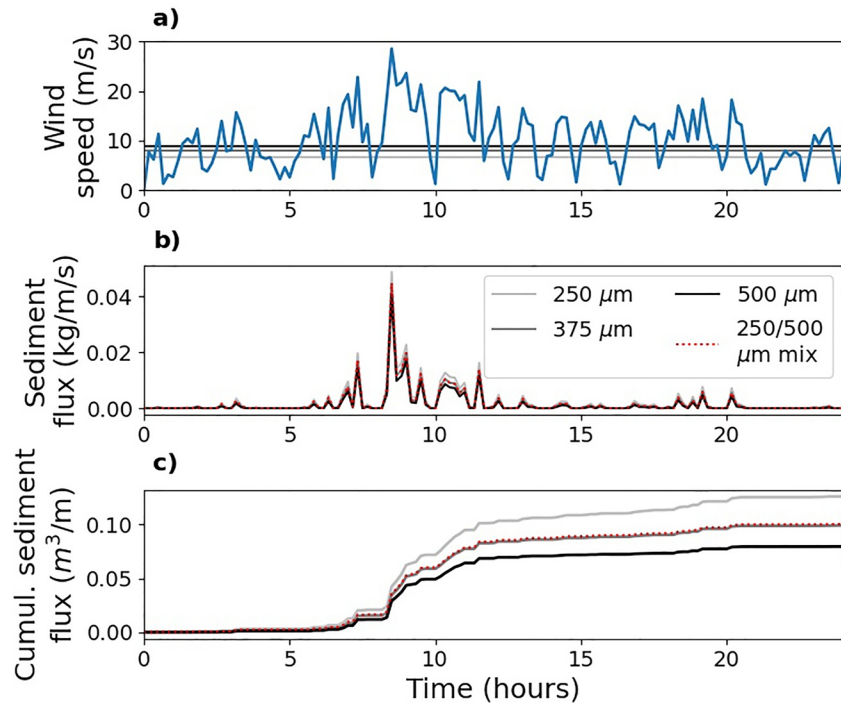
Figure 6. (a) One-day variable wind scenario which results in the (b) sediment flux and (c) cumulative sediment flux of the single-fraction cases of 250, 375, and 500 μm and of a two-fraction 250/500 μm mix (50%–50% mix, Figure 3b). The horizontal lines in the wind plot indicate the threshold velocity for the single-fraction case with the corresponding color in (b) and (c).

(Figure 6c), which is the result of both the difference in threshold velocity and the transport magnitude. For finer grain sizes, the lower threshold velocity resulted in a longer time period in which transport could occur, and in that time period, the transport was higher than that for the coarser grain sizes (Figure 6a).

4.2. Comparison Between Single-Fraction and Two-Fraction Mixes

The 50%–50% mix with the 250 and 500 μm sediment fractions resulted in similar transport rates as the single-fraction simulation with the average grain size of 375 μm (Figure 6c). For the simulated wind climate, there was little effect of the coarsening of the top layer. There was some differentiation between the mix and the 375 μm case in periods where the wind speed was between the threshold velocity of the 250 and 500 μm fractions. This differentiation occurred around relatively low wind speeds of 6.7–9.0 m/s, which caused the absolute difference between the sediment transport of the two fractions to be small (6.5×10^{-5} m³/m at 9 m/s over 10 min, Figure 5a). This small difference does not result in coarsening in the simulation because it does not have a significant effect on the composition of the surface grid cells. Additionally, the highest wind speeds resulted in the largest contribution to the sediment flux. Thus, the differentiation at lower wind speeds was negligible on the scale of the total cumulative sediment flux during the 1-day simulation. At higher wind speeds, the sediment transport of the 250 μm fraction was larger than that of the 375 μm fraction at a similar magnitude as the sediment transport of the 500 μm fraction was smaller than the 375 μm fraction (Figure 5a). The larger and smaller transport that occurred, respectively, for the 250 and 500 μm fractions in the mix balanced each other, making the resulting cumulative transport comparable to the 375 μm case. At the yearly time scale, the behavior of the two-fraction mix was also closely replicated with a single fraction equal to the average grain size of the mix.

The effect of armoring was further investigated with 80%–20% mixes of varying grain sizes (125/2,000 μm, 300/1,300 μm, and 375/1,000 μm) with a constant average grain size equal to 500 μm. At a yearly timescale, the cumulative sediment flux varied for the different mixes (Figure 7). The 375/1,000 μm case aligned with the result of the average grain size, the 300/1,300 μm mix was slightly larger, and the 125/2,000 μm mix showed larger deviations. At the start of the year, the cumulative sediment flux of the 125/2,000 μm mix exceeded that of the
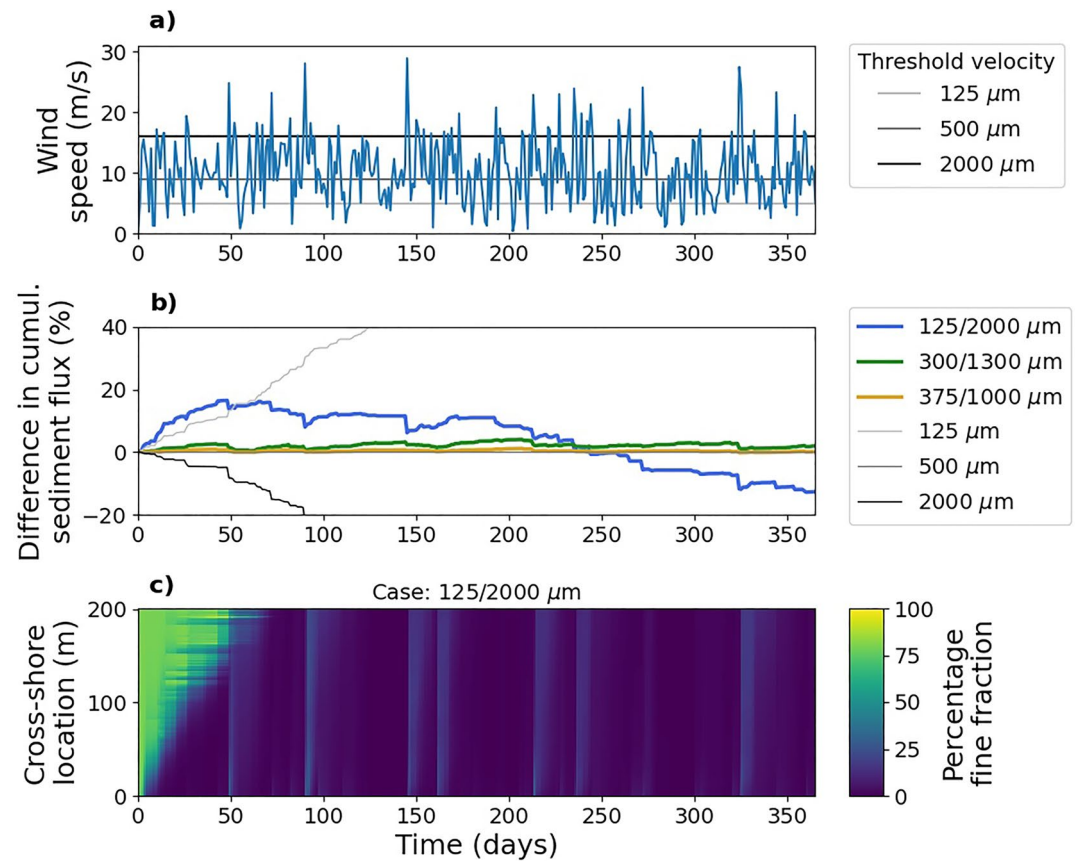
Figure 7. (a) 1-year variable wind scenario. The horizontal lines in the wind plot indicate the threshold velocity for single-fraction cases with colors corresponding to the sediment fluxes in (b). (b) Cumulative sediment flux of the single-fraction cases of 125 μm (light gray), 500 μm (gray), and 2,000 μm (black), compared to the cumulative sediment flux that occurs for 80%–20% mixes (Figure 3c) in blue, green, and yellow that all have an average grain size of 500 μm. Note that the single-fraction case of 500 μm is used as the reference case. (c) Time-stack of the development of the percentage of fine fraction that is present in the top layer of the bed surface for the 125/2,000 μm mix through time (x-axis) and space (y-axis).

average grain size. Within the first 50 days, it even exceeded the cumulative sediment flux of the single-fraction 125 μm case. The explaining mechanism is the increase of the aerodynamic roughness in the mix that was caused by the coarse fraction. A larger aerodynamic roughness increases the shear velocity (greyscale lines in Figure 5b) and, thus, the transport capacity, which is dependent on the difference between the shear velocity and the threshold shear velocity (Equation 1). After the 50-day period, this increased transport capacity was counteracted by the coarsening of the bed surface (Figure 7c), and the cumulative sediment flux progressively got closer to the reference case. This effect of coarsening on the difference in cumulative sediment flux was sustained during wind speed peaks despite the exposure of more fine fraction when erosion of the coarse top layer occurred (e.g., Figure 7c, day 145). During these wind speed peaks, both the fine and coarse fraction could be transported; however, the large amount of 2,000 μm fraction in the mix caused less transport to occur than for the reference of 500 μm (following the trend of lower fluxes for larger grain sizes as shown in Figure 5a). After 240 days, the cumulative transport of the 125/2,000 μm case became even lower than the reference case, eventually resulting in approximately 15% less cumulative transport at the end of the year. Similar fluctuations in the difference in cumulative sediment flux occurred for the 300/1,300 μm mix, although the cumulative sediment flux was never less than the reference case.

4.3. The Effect of Coarse Fraction Percentage on Sediment Transport

Not only the size but also the relative percentage of the coarse fraction affects the cumulative sediment flux (Figure 8). The effect of the percentage of coarse fraction was investigated by varying the coarse sediment
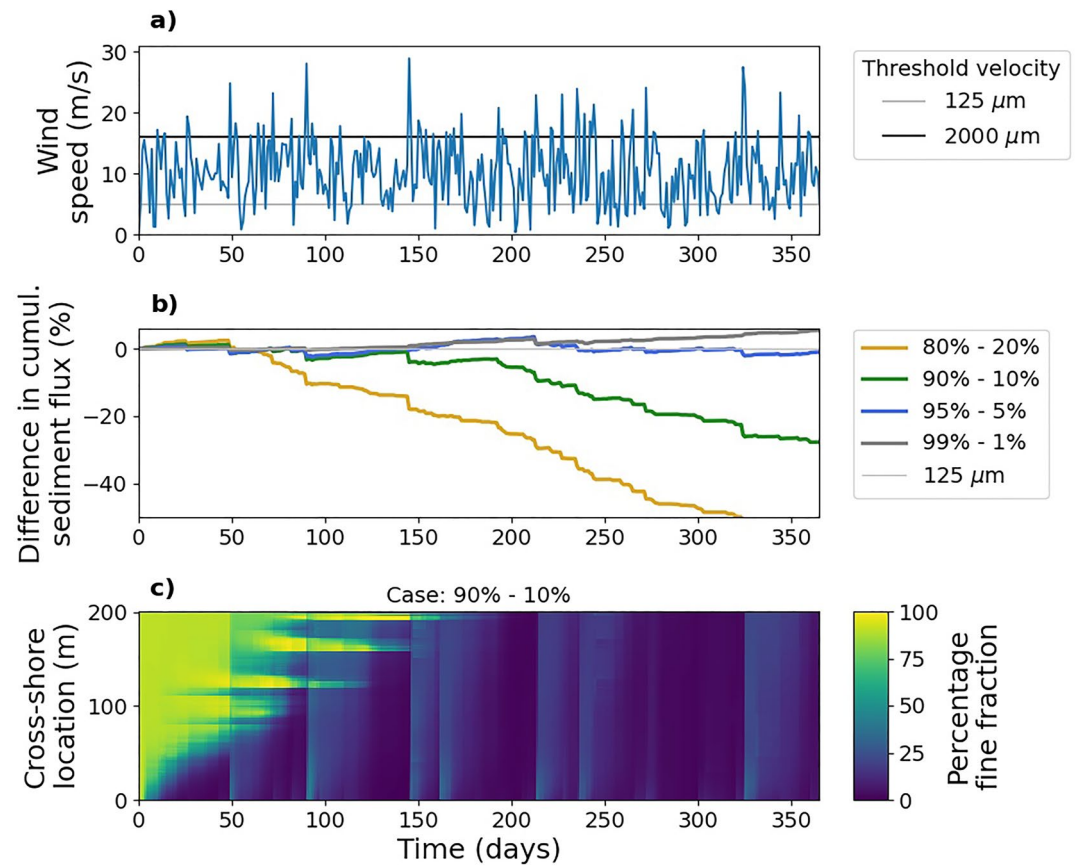
Figure 8. (a) 1-year variable wind scenario. The horizontal lines in the wind plot indicate the threshold velocity for the single-fraction case of 125 μm (light gray) and 2,000 μm (black). (b) Cumulative sediment flux of the reference single-fraction case of 125 μm (light gray), compared to the cumulative sediment flux that occurs for two-fraction mixes in yellow, green, blue, and gray that consist of varying percentages of the 125 and 2,000 μm fractions (Figure 3d). (c) Time-stack of the development of the percentage of fine fraction that is present in the top layer of the bed surface through time (*x*-axis) and space (*y*-axis), visualized for the 125/2,000 μm mix that starts with 90% fine and 10% coarse fraction.

percentage between 1% and 20% in a 125/2,000 μm mix (Figure 3d). The 80%–20% case showed a strong deviation in the cumulative sediment flux compared to the reference case (100% 125 μm) resulting in a decrease in the yearly cumulative transport rate of more than 50% (Figure 8b). The decrease in transport due to armoring occurred from 70 days and onward. For the 90%–10% case, it took 150 days for this deviation to occur, and the deviation after a year was smaller, at approximately 30% less transport than the reference case. The cases where only 1 or 5% of the coarse fraction was present did not show a considerable deviation from the sediment flux of the fine fraction within the 1-year time frame. All cases showed how wind speed peaks affect the cumulative sediment flux. The wind speed peaks cause mobilization of the coarse fraction at the bed surface, which exposes finer fractions that are more easily transported (Figure 8c).

4.4. The Effect of Different Particle Size Distributions on Sediment Transport

Compared to the two fraction mixes, the simulations with full PSDs resulted in less deviation from the reference case (median grain size of the PSD). The maximum difference in cumulative sediment flux was 15% and 7.5% less transport after the 1-day (Figure 9) and 1-year period (Figure 10), respectively. Overall, all PSDs showed comparable trajectories, except for PSD 6, which has the widest distribution. In the 1-day period, PSD 6 showed several hours with a larger cumulative sediment flux than the reference grain size. This might have been related to a relatively large aerodynamics roughness and fine fraction abundance, caused by the shape of PSD 6 (Figure 3e). In the 1-year period, PSD 6 remained relatively close to the reference grain size up until day 200, whereas the other PSDs already showed significant deviations near the start of the simulation. Again, this behavior might be caused by the balance between the presence of coarse and fine fractions in the grain-size distribution.
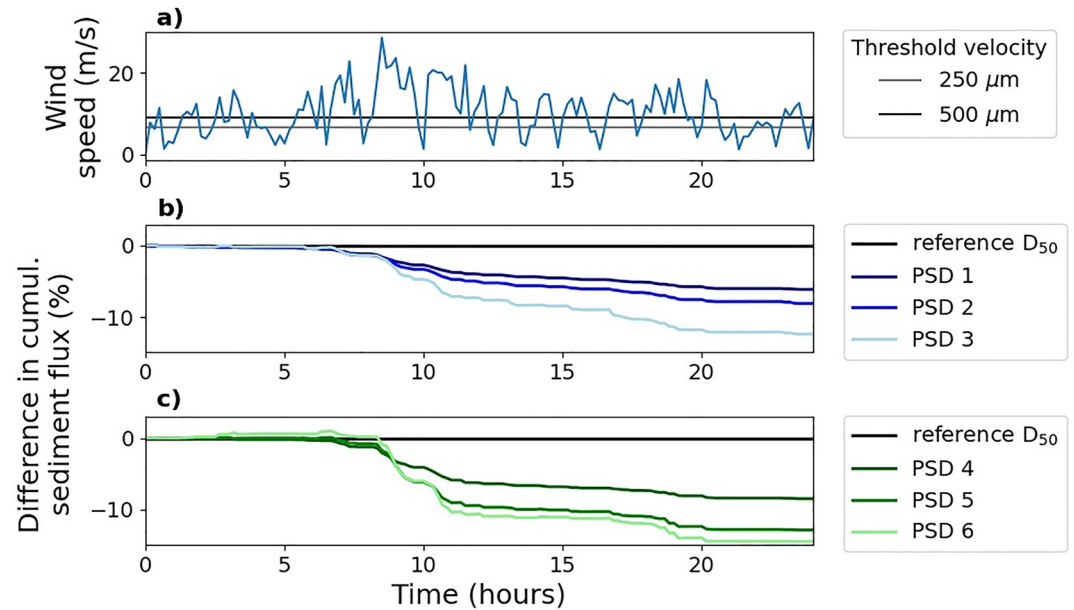
Figure 9. (a) 1-day variable wind scenario. The horizontal lines in the wind plot indicate the threshold velocity for the single-fraction case of 250 μm (gray) and 500 μm (black). (b) and (c) Cumulative sediment flux of each tested particle size distribution (PSD) as shown in Figure 3e, compared to the reference case (black). For each PSD, the reference case corresponds to the median grain size of the PSD. The blue colors in (b) have a median grain size of around 250 μm, the green colors in (c) have a median grain size around 500 μm.

4.5. The Impact of Grain-Size Variability in the Horizontal Dimension

The horizontal variation cases with different spatial gradients showed distinctly different cumulative sediment fluxes when simulated for a 10-min period with a constant 10 m/s speed. The finer the sediment at the start of
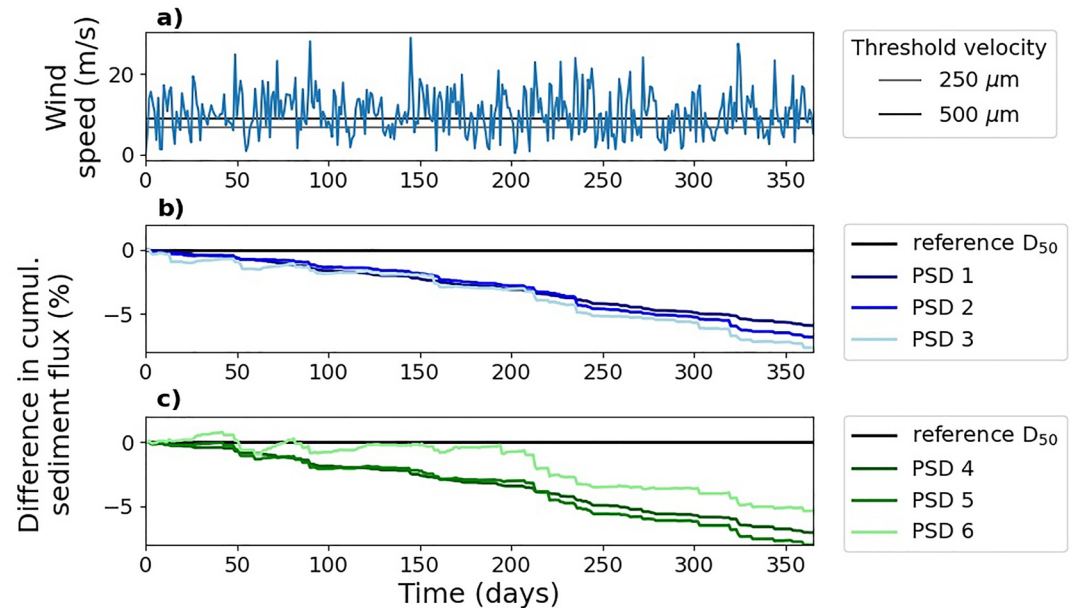

Figure 10. (a) 1-year variable wind scenario. The horizontal lines in the wind plot indicate the threshold velocity for the single-fraction case of 250 μm (gray) and 500 μm (black). (b) and (c) Cumulative sediment flux of each tested particle size distribution (PSD) as shown in Figure 3e, compared to the reference case (black). For each PSD, the reference case corresponds to the median grain size of the PSD. The blue colors in (b) have a median grain size of around 250 μm, the green colors in (c) have a median grain size around 500 μm.
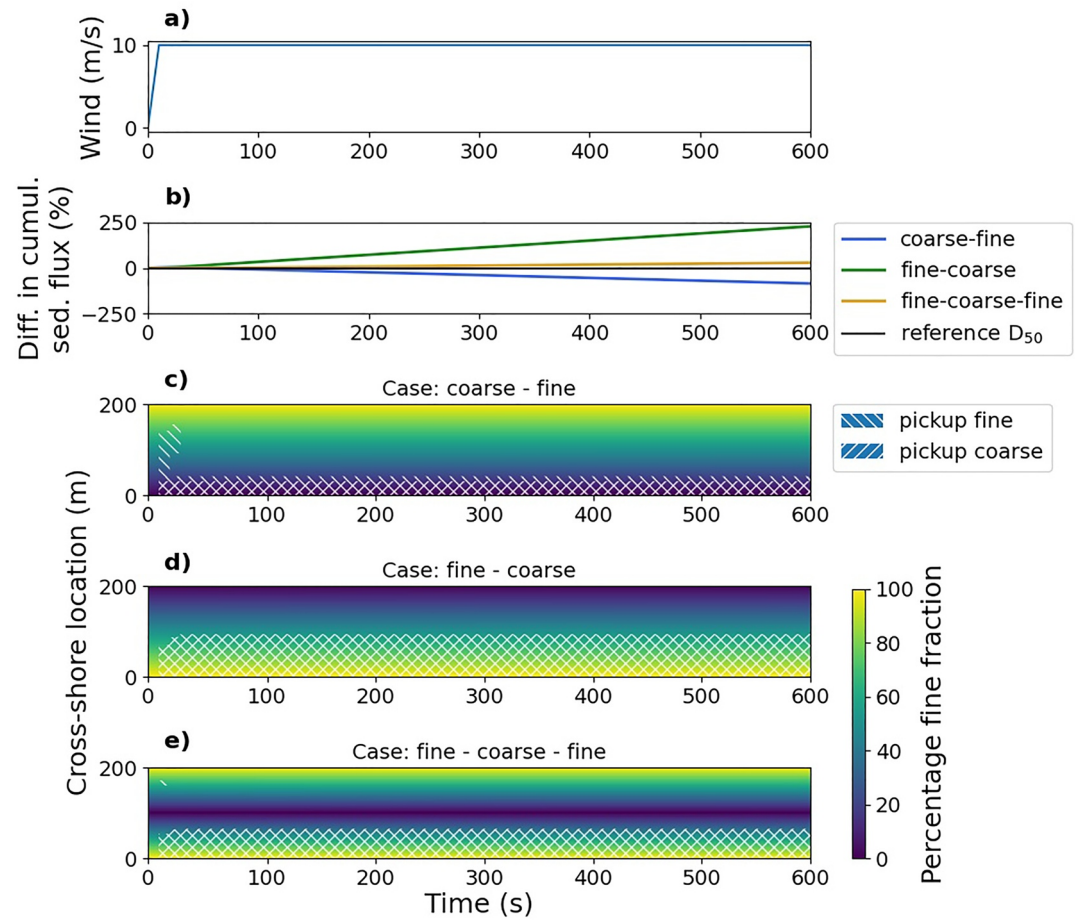
Figure 11. (a) Cumulative sediment fluxes under a 10-min, constant 10 m/s wind speed for the horizontal variation scenario (Figure 4a), which includes a coarse to fine (blue), fine to coarse (green) and fine to coarse to fine (yellow) gradient, compared to the reference grain size of 375 μm (black). Time-stack of the development of the percentage of fine fraction that is present in the top layer of the bed surface for the (b) coarse to fine, (c) fine to coarse and (d) fine to coarse to fine cases.

the domain, the higher the cumulative sediment flux (Figure 11). In Figures 11b–11d, the erosion area in the domain is indicated with white hatching, where leftward leaning hatching indicates pickup of the fine fraction and rightward leaning hatching indicates the pickup of the coarse fraction. The variation in the cross-shore expanse of the erosion area between the different scenarios indicates a variation in the fetch length, which could have been caused by a difference in the magnitude of the equilibrium transport. Coarse sediment resulted in a lower equilibrium transport magnitude (Equation 1); therefore, based on the implementation of the adaptation timescale, the distance needed to reach the equilibrium transport was smaller than with fine sediment at the start of the domain, which is related to a larger equilibrium transport. The larger bed roughness that occurred for the coarse sediment counteracted this effect slightly. In conclusion, the fetch length in these simulations is shorter when coarser sediment is present at the start of the domain, and as fully developed transport was reached at the end of the erosion area, there was no significant impact of the bed surface gain size composition further along the domain.

The 1-day and 1-year simulations of the horizontal grain-size variations resulted in similar sediment flux behavior. The coarse-fine case resulted in less transport than the reference D_{50} and the fine-coarse and fine-coarse-fine cases resulted in more transport (Figure 12). The bed surface layer development of the coarse-fine case showed coarsening of the surface (Figure 12c), whereas the fine-coarse case showed fining (Figure 12d). For each case, a unique cross-shore equilibrium bed composition developed at the bed surface. The occurrence of pickup throughout the domain seemed to be most strongly related to the wind speed. However, after the formation of the equilibrium grain-size gradient, the region with pickup became much larger for both periods and all cases.
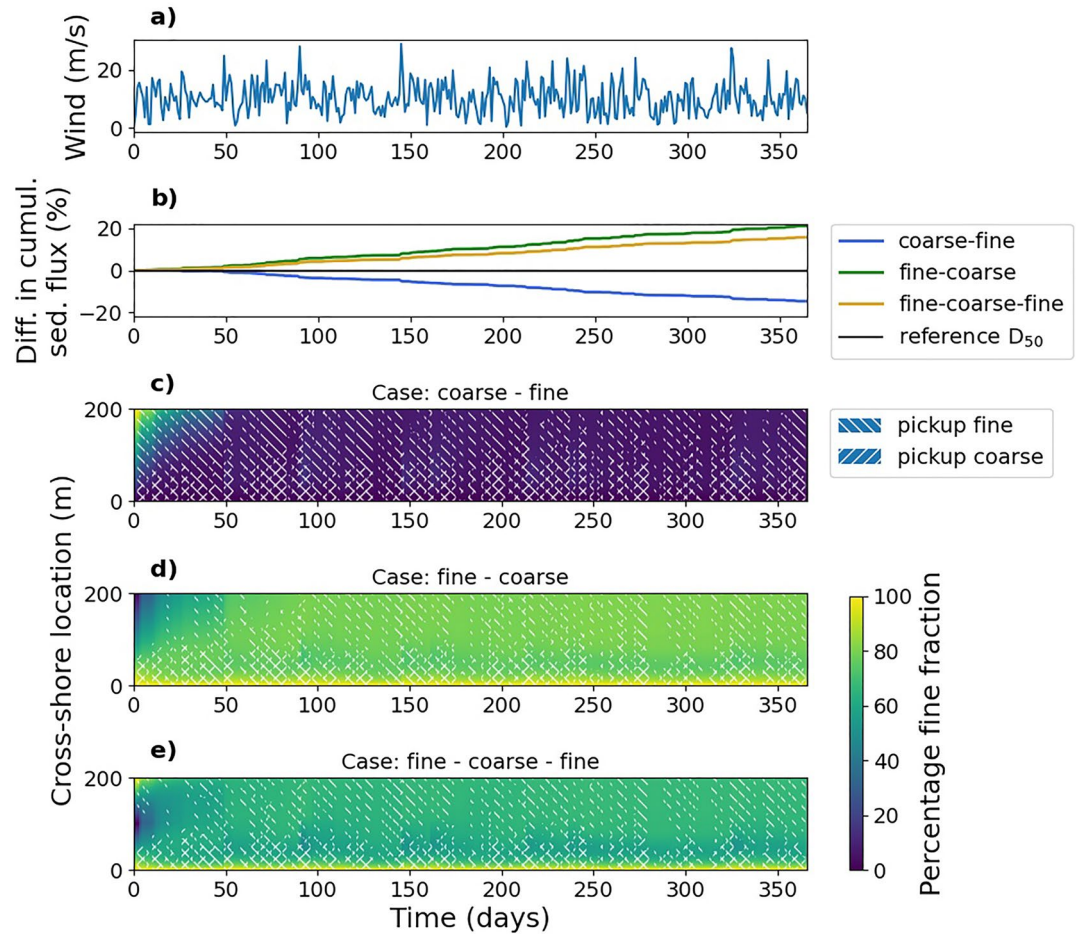
Figure 12. (a) 1-year variable wind scenario. (b) Cumulative sediment fluxes of the horizontal variation scenario (Figure 4a), which includes a coarse to fine (blue), fine to coarse (green) and fine to coarse to fine (yellow) gradient, compared to the reference grain size of 375 μm (black). Time-stack of the development of the percentage of fine fractions that is present in the top layer of the bed surface for the (b) coarse to fine, (c) fine to coarse and (d) fine to coarse to fine cases.

4.6. Sediment Transport Variations Due To Vertical Grain-Size Variability

The vertical grain-size layering directly affected the amount and timing of aeolian transport during the different time scales. For the 10-min simulations, varying behavior was observed depending on the wind speed and the vertical location of the coarse layer (Figure 13). At a wind speed of 10 m/s, little transport occurred due to the relatively low wind speeds, and the grain-size fraction in the upper layer of both cases dominated the cumulative sediment flux (Figure 13a). At 20 m/s, the removal of the coarse and fine fraction for the 1st layer coarse and 4th layer coarse case, respectively, resulted in a reduction of the difference in the cumulative sediment flux compared to the reference grain size (Figure 13b). At 30 m/s, both the fine and coarse sediments were easily mobilized by the wind, resulting in a considerably lower difference in cumulative sediment flux compared to the reference grain size (Figure 13c).

On the scale of a 1-day simulation, the main differentiation in the cumulative sediment flux between the vertical layering cases and the reference grain size (Figure 14b) occurred during the wind peak between hours 5 and 10 (Figure 14a). This wind peak caused the coarse and fine sediment of, respectively, the 1st coarse case and 4th coarse case to be removed from the surface layer (Figures 14c and 14d). Subsequently, a relatively stable spatial grain-size gradient formed, and the difference in cumulative sediment flux showed limited change for both cases. As the spatial grain-size gradient of the bed surface layer changed, the extent of the pickup area, especially for the coarse fraction, increased. Overall, the 1-year simulation showed comparable trends to the 1-day simulation, although the difference in cumulative sediment flux compared to the reference was lower (around 1% vs. 5%).
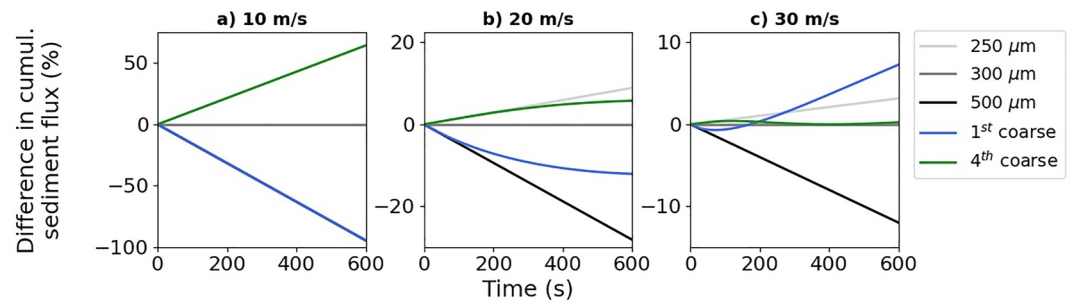
Figure 13. Cumulative sediment fluxes of the vertical layering scenario (Figure 4b) compared to the reference grain size 300 μm (gray) for 10-min simulations with a constant wind speed of (a) 10 m/s, (b) 20 m/s, and (c) 30 m/s. The scenario includes the case where the top layer (blue) and the fourth layer (green) consisted of a coarse fraction (500 μm). The other layers consisted of a fine fraction (250 μm). For comparison, the cumulative sediment flux of the single-fraction case of 250 (light gray) and 500 μm (black) are shown.
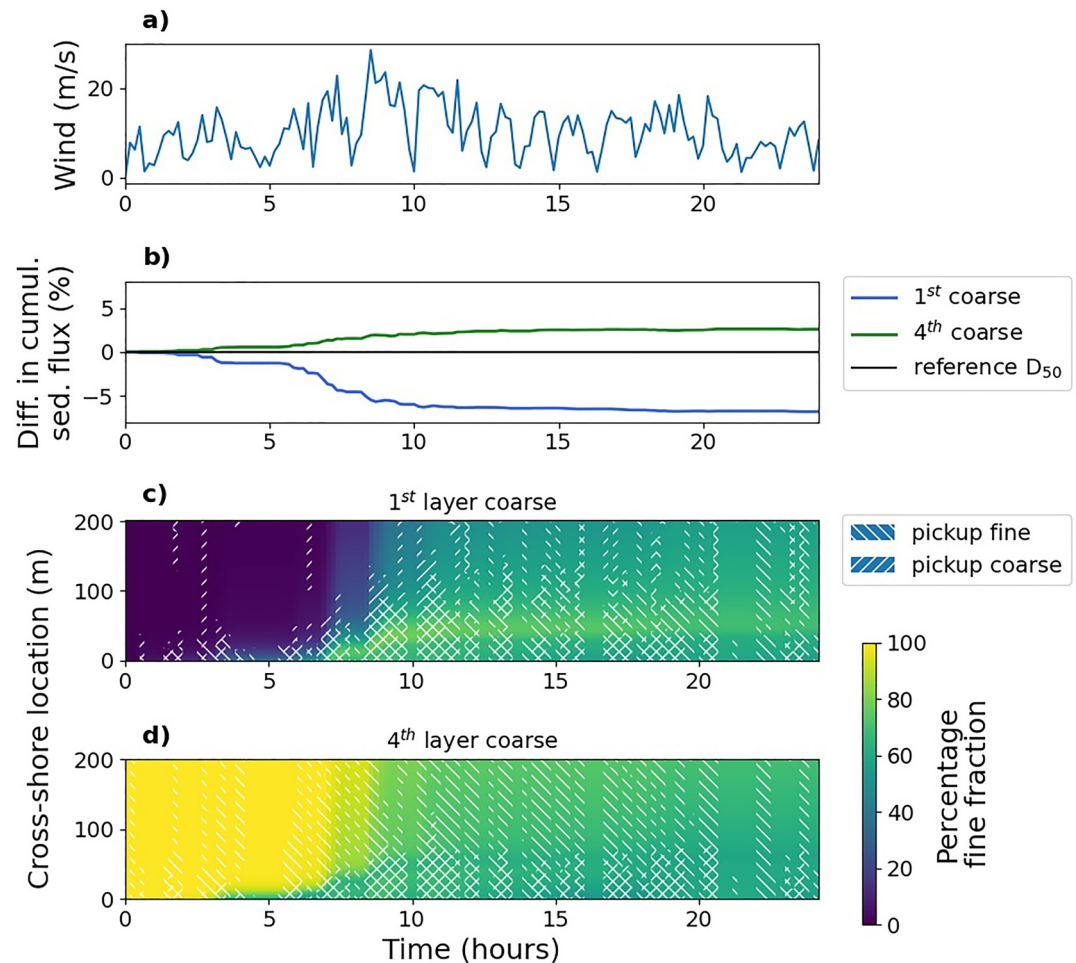
Figure 14. (a) 1-day variable wind scenario. (b) Cumulative sediment fluxes of the vertical layering scenario (Figure 4b) compared to the reference grain size 300 μm (black). The scenario includes case 1 (blue), where the top layer consisted of a coarse fraction, and case 2 (green), where the fourth layer consisted of a coarse fraction (500 μm). The other layers consisted of a fine fraction (250 μm). Time-stack of the development of the percentage of fine fractions that is present in the top layer of the bed surface for (b) case 1 and (c) case 2.

5. Discussion

5.1. Using a Single-Fraction Representative Grain Size in Aeolian Sediment Transport Modeling

We hypothesized that the inclusion of multi-fraction transport in aeolian sedimen transport simulations would have a considerable effect on the calculated sediment transport. However, the cumulative sediment flux calculated using multi-fraction transport and its approximation with a single-fraction reference grain size were similar on time scales of days to years. There was only a considerable impact on the yearly cumulative transport when a relatively large content of coarse grains, >10% of 2,000 μm sediment, was present. The full PSD scenarios, which are similar to the grain-size distribution of beach sand, resulted in a maximum transport reduction of 15% over 1 day and 7.5% over 1 year compared to the median grain size. These values are in a similar order of magnitude as those found by Hoonhout and de Vries (2016), although the presence of shells further exacerbated the resulting reduction in their study. The results indicate that for most scenarios, the median grain size can be used as a pragmatic metric for natural grain-size distributions in aeolian sediment transport models at daily to yearly time scales.

There are some limitations to simplifying grain-size distributions with the median grain size. In some of the single-fraction simulations, larger transport rates were recorded than in the corresponding multi-fraction simulation. Wide PSDs might include a relatively large contribution of both coarse and fine fractions. The fine fraction abundance may result in a relative increase of total transport compared to narrower PSDs (e.g., PSD 6 compared to PSD 4 and 5 in Figure 10). Additionally, several multi-fraction cases showed that increased transport can occur in the model despite an increase in the reference grain size (e.g., the 125/2,000 μm mix in Figure 7). This simulated sediment transport increase is related to an increase in the bed roughness and the shear velocity (Equation 3). In all cases, the effect was temporary, as coarsening due to the removal of fines counteracted the increase in transport caused by the roughness.

The suitability of the D_{50} as a representative grain size can also be affected by armoring that limits the aeolian sediment transport. These armoring effects occur when a considerable amount of coarse grains is present. Whether specific grain sizes will result in armoring depends on the local wind climate. During energetic wind events, wind peaks can cause an increase in sediment transport and mobilization of coarse grains from the bed surface, which can expose underlying sediment (e.g., the 125/2,000 μm mix in Figure 7). For the synthetic wind climate that was generated and used in this study, about 2,000 μm was a critical grain size. Future work could further quantify, both for coastal settings and other aeolian settings such as deserts, for which wind climates and grain-size distributions the use of the D_{50} as a representative grain size is valid. For now, a representative wind forcing could be created based on the wind climate and used in an aeolian sediment transport model to determine the extent to which specific coarse fractions are expected to be mobilized.

Besides wind speed peaks, hydrodynamic processes and trampling can also break up and alter armor layers. Hydrodynamic processes can cause erosion, deposition and mixing that directly affect the top layers of the bed surface on a time scale of seasons (e.g., Abuodha, 2003; Prodger et al., 2017), events (e.g., Gallagher et al., 2016) and tides (e.g., van IJzendoorn et al., 2022). Future work could investigate the effect of temporally varying grain sizes due to hydrodynamic processes on the sediment flux by including temporal grain-size variations in modeling simulations by making simplified assumptions (e.g., based on findings by van IJzendoorn et al. (2022)) or coupling with a numerical model (Reniers et al., 2013; Srisuwan & Work, 2015). Trampling is also expected to affect the grain size at the bed surface (Moayeri et al., 2023; Reyes-Martínez et al., 2015). Its effects could be included in aeolian sediment transport models with mixing of surface layers in locations where human activity is expected.

5.2. The Implementation of Spatial Grain-Size Variations in Aeolian Sediment Transport Modeling

Significant vertical grain-size variations at the bed surface have been measured (e.g., van IJzendoorn et al., 2022) and over larger soil depths (e.g., Gallagher et al., 2016; Gunaratna et al., 2019). The measurements of van IJzendoorn et al. (2022) showed a maximum range of 119 μm in the D_{50} of different layers in the top 5 cm of the bed surface. Based on our results, we expect that these variations could be simulated relatively accurately on the daily and yearly timescales with the D_{50}. This is contrary to our hypothesis that spatial grain-size variations would have a considerable effect on calculated sediment transport. However, on the minute-scale, we expect that the sediment flux could significantly be altered, especially when layers with a significant contribution of coarse fraction are present near the bed surface. We recommend the inclusion of vertical grain-size layering in aeolian sediment transport models where short-term time scales are considered. On time scales longer than days, they can be omitted.

The source area at the beginning of the domain has a significant impact on the cumulative sediment flux across all time scales. As a result, there can be a disconnect between the grain size that is at the bed surface and the transport that occurs at that location. Consider a point measurement at the end of the domain of the coarse—fine and fine—coarse—fine cases for the 10-min time scale (Figure 13). The grain size at these locations was comparable, but the cumulative sediment flux deviated considerably. This difference was mostly related to the grain size of the material present in the source area where pickup of fine and coarse sediment occurred. This shows that it is important to consider the grain size that is present in the source area when explaining minute-scale sediment transport measurements, as previously indicated by Cohn et al. (2022), Field and Pelletier (2018), and Uphues et al. (2022). These grain-size measurements should be recent because wind speed peaks can cause temporal variations in the bed surface grain size and the related aeolian sediment transport.

The intertidal area was found to be an important source for aeolian sediment transport toward the dunes by de Vries, Arens, et al. (2014). Our findings show that this upwind source of sediment is important for the bed surface grain-size development across the domain and the sediment transport magnitude. Thus, the results suggest that the grain size in the intertidal area (e.g., Bascom, 1951) might be the most important to include in aeolian sediment transport models that are used for coastal dune development predictions. These findings align with measurements of aeolian sediment transport in the intertidal area by Swann et al. (2021), who found similar grain sizes in the air column as on the bed. Future work could further validate or falsify these findings by combining minute-scale quantitative sediment transport measurements with bed surface grain-size measurements that can show a temporal variation through time. Furthermore, the importance of the grain size in the intertidal area emphasizes the need to study sediment supply by hydrodynamic processes and, specifically, its effect on grain-size composition.

5.3. The Implementation of Small-Scale Physics in Aeolian Sediment Transport Modeling

Besides the implementation of hydrodynamic processes, the validity of the implementation of small-scale, grain-size related physical processes in the model (Figure 1) compared to the functioning of these physical processes in the field remains uncertain. For example, the effect of the bed roughness, the relation between grain size and fetch length, and the time scale at which coarsening occurs remain unknown. In the current work, a main assumption is that $\sqrt{\frac{d}{D}}$ in the Bagnold equation (Equation 1) is equal to 1. This assumption was made in accordance with Hoonhout and de Vries (2016) because the effect of grain size on the sediment transport rate is implemented through the threshold shear velocity. However, based on Equation 1, it could be argued that using a different definition of $\sqrt{\frac{d}{D}}$ might impact the conclusions of the present work. Therefore, we tested the sensitivity of the model simulations to a different implementation of this term. Results presented in Figures S1–S6 of the Supporting Information S1 show several model simulations from the current work that were re-calculated using the Bagnold equation where $\sqrt{\frac{d}{D}}$ is calculated based on the grain size of each individual grain-size fraction.

These results show that at a 10-min time scale the sediment transport behavior of the grain-size fractions changes for the higher wind speeds (Figure S1 in Supporting Information S1). However, on longer time scales behavior can vary slightly, but the overall trends seen in the results remain the same. This emphasizes that, depending on the wind speed, small-scale physics and the determination of grain size can be important on a short time scale, but that the D_{50} is a suitable reference grain size on longer time scales. It is still uncertain which methods to implement small-scale, grain-size related physics in aeolian sediment transport modeling provide the most reliable description, especially in the case of multi-fraction transport. We expect that the output of bed surface grain size and sediment transport information by the model may inspire detailed comparison to field or lab measurements in future work, which, in turn, could improve the implementation of small-scale physics in the model.

6. Conclusions and Recommendations

The sorting of multi-fraction sediment, spatial variations in grain size, and their impact on aeolian sediment transport were studied using a numerical aeolian sediment transport model. Results show that, in general, the D_{50} can be used as a representative grain size in aeolian sediment transport modeling on a time scale of days to years. For wide grain-size distributions, the multi-fraction sediment flux may differ from the single-fraction flux of the reference grain size. In these cases, simplified model runs that include the full PSD and a wind forcing representative for the wind climate to test the impact on the sediment flux could be considered.

On a time scale of 10-min, the bed surface grain size has a direct effect on the aeolian sediment transport flux. Due to this strong relation between grain size and sediment transport, vertical grain-size layering may be required in models that predict aeolian sediment transport at this time scale. On time scales from days to years, modeling the effect of vertical layering may not be needed if a representative grain size is used.

The effect of horizontal grain-size variations is relevant across all time scales. The grain size in the upwind part of the domain can directly affect the transport magnitude across the domain. The intertidal area can be the dominant source of aeolian sediment transport that affects coastal dune development. In these cases, we recommend to include the grain size present in this region in aeolian sediment transport models and consider its impact on point measurements of sediment transport recorded on the beach. Additionally, we recommend to further investigate the supply of sediment to the intertidal zone by marine processes, specifically focusing on grain size.

Data Availability Statement

Version 2.1.0 of the AeoLiS software used for the aeolian sediment transport simulations in this research is preserved at https://doi.org/10.4121/22215562, available via GPL-3.0 and developed openly on Github (https://github.com/openearth/aeolis-python). The Python code used for the analysis and figure generation is hosted at Github (https://github.com/christavanijzendoorn/grainsizeanalysis-aeolis) and is preserved at https://doi.org/10.4121/22220134, version 1.1.0, under GPL-3.0.

References

Abuodha, J. O. Z. (2003). Grain size distribution and composition of modern dune and beach sediments, Malindi Bay coast, Kenya. *Journal of African Earth Sciences*, *36*(1–2), 41–54. https://doi.org/10.1016/S0899-5362(03)00016-2

Anderson, R. S., & Haff, P. K. (1988). Simulation of eolian saltation. *Science*, *241*(4867), 820–823. https://doi.org/10.1126/SCIENCE.241.4867.820

Bagnold, R. A. (1937a). The size-grading of sand by wind. *Proceedings of the Royal Society of London. Series A—Mathematical and Physical Sciences*, *163*(913), 250–264. https://doi.org/10.1098/rspa.1937.0225

Bagnold, R. A. (1937b). The transport of sand by wind. *The Geographical Journal*, *89*(5), 409. https://doi.org/10.2307/1786411

Bascom, W. N. (1951). The relationship between sand size and beach-face slope. *Eos, Transactions American Geophysical Union*, *32*(6), 866–874. https://doi.org/10.1029/TR032I006P00866

Bauer, B. O. (1991). Aeolian decoupling of beach sediments. *Annals of the Association of American Geographers*, *81*(2), 290–303. https://doi.org/10.1111/j.1467-8306.1991.tb01691.x

Bauer, B. O., & Davidson-Arnott, R. G. D. (2002). A general framework for modeling sediment supply to coastal dunes including wind angle, beach geometry, and fetch effects. *Geomorphology*, *49*(1–2), 89–108. https://doi.org/10.1016/S0169-555X(02)00165-4

Bristow, N. R., Best, J., Wiggs, G. F. S., Nield, J. M., Baddock, M. C., Delorme, P., & Christensen, K. T. (2022). Topographic perturbation of turbulent boundary layers by low-angle, early-stage aeolian dunes. *Earth Surface Processes and Landforms*, *47*(6), 1439–1454. https://doi.org/10.1002/ESP.5326

Çelikoglu, Y., Yüksel, Y., & Sedat Kabdaşli, M. (2006). Cross-shore sorting on a beach under wave action. *Journal of Coastal Research*, *22*(3), 487–501. https://doi.org/10.2112/05-0567.1

Cheng, H., He, J., Zou, X., Li, J., Liu, C., Liu, B., et al. (2015). Characteristics of particle size for creeping and saltating sand grains in aeolian transport. *Sedimentology*, *62*(5), 1497–1511. https://doi.org/10.1111/SED.12191

Cohn, N., Dickhudt, P., & Marshall, J. (2022). In situ measurement of grain size characteristics within the aeolian saltation layer on a coastal beach. *Earth Surface Processes and Landforms*, *47*(9), 2230–2244. https://doi.org/10.1002/ESP.5373

Delgado-Fernandez, I. (2010). A review of the application of the fetch effect to modelling sand supply to coastal foredunes. *Aeolian Research*, *2*(2–3), 61–70. https://doi.org/10.1016/j.aeolia.2010.04.001

de Vries, S., Arens, S. M., de Schipper, M. A., & Ranasinghe, R. (2014). Aeolian sediment transport on a beach with a varying sediment supply. *Aeolian Research*. https://doi.org/10.1016/j.aeolia.2014.08.001

de Vries, S., Hallin, C., van IJzendoorn, C., van Westen, B., Cohn, N., Strypsteen, G., et al. (2023). AeoLiS (version v2.1.0) [Software]. 4TU Repository. https://doi.org/10.4121/22215562

de Vries, S., van Thiel de Vries, J. S. M., van Rijn, L. C., Arens, S. M., & Ranasinghe, R. (2014). Aeolian sediment transport in supply limited situations. *Aeolian Research*, *12*, 75–85. https://doi.org/10.1016/j.aeolia.2013.11.005

Dong, Z., Wang, H., Liu, X., & Wang, X. (2004). A wind tunnel investigation of the influences of fetch length on the flux profile of a sand cloud blowing over a gravel surface. *Earth Surface Processes and Landforms*, *29*(13), 1613–1626. https://doi.org/10.1002/esp.1116

Durán, O., Claudin, P., & Andreotti, B. (2011). On aeolian transport: Grain-scale interactions, dynamical mechanisms and scaling laws. *Aeolian Research*, *3*(3), 243–270. https://doi.org/10.1016/J.AEOLIA.2011.07.006

Edwards, A. C. (2001). Grain size and sorting in modern beach sands. *Journal of Coastal Research*, *17*(1).

Field, J. P., & Pelletier, J. D. (2018). Controls on the aerodynamic roughness length and the grain-size dependence of aeolian sediment transport. *Earth Surface Processes and Landforms*, *43*(12), 2616–2626. https://doi.org/10.1002/ESP.4420

Gallagher, E. L., Wadman, H., McNinch, J., Reniers, A., & Koktas, M. (2016). A conceptual model for spatial grain size variability on the surface of and within beaches. *Journal of Marine Science and Engineering*, *4*(2), 38. https://doi.org/10.3390/JMSE4020038

Gao, X., Narteau, C., & Rozier, O. (2016). Controls on and effects of armoring and vertical sorting in aeolian dune fields: A numerical simulation study. *Geophysical Research Letters*, *43*(6), 2614–2622. https://doi.org/10.1002/2016GL068416

Gillette, D. A., Herbert, G., Stockton, P. H., & Owen, P. R. (1996). Causes of the fetch effect in wind erosion. *Earth Surface Processes and Landforms*, *21*(7), 641–659. https://doi.org/10.1002/(SICI)1096-9837(199607)21:7

Gunaratna, T., Suzuki, T., & Yanagishima, S. (2019). Cross-shore grain size and sorting patterns for the bed profile variation at a dissipative beach: Hasaki Coast, Japan. *Marine Geology*, *407*, 111–120. https://doi.org/10.1016/J.MARGEO.2018.10.008

Hallin, C., Almström, B., Larson, M., & Hanson, H. (2019). Longshore transport variability of beach face grain size: Implications for dune evolution. *Journal of Coastal Research*, *35*(4), 751–764. https://doi.org/10.2112/JCOASTRES-D-18-00153.1

Hallin, C., Huisman, B. J. A., Larson, M., Walstra, D. J. R., & Hanson, H. (2019). Impact of sediment supply on decadal-scale dune evolution—Analysis and modelling of the Kennemer dunes in the Netherlands. *Geomorphology*, *337*, 94–110. https://doi.org/10.1016/j.geomorph.2019.04.003

Hallin, C., Larson, M., & Hanson, H. (2019). Simulating beach and dune evolution at decadal to centennial scale under rising sea levels. *PLoS One*, *14*(4), e0215651. https://doi.org/10.1371/journal.pone.0215651

Hoonhout, B., & de Vries, S. (2016). A process-based model for aeolian sediment transport and spatiotemporal varying sediment availability. *Journal of Geophysical Research: Earth Surface*, *121*(8), 1555–1575. https://doi.org/10.1002/2015JF003692

Hoonhout, B., & de Vries, S. (2019). Simulating spatiotemporal aeolian sediment supply at a mega nourishment. *Coastal Engineering*, *145*, 21–35. https://doi.org/10.1016/j.coastaleng.2018.12.007

Houser, C. (2009). Synchronization of transport and supply in beach-dune interaction. *Progress in Physical Geography*, *33*(6), 733–746. https://doi.org/10.1177/0309133309350120

Kroon, A., de Schipper, M., de Vries, S., & Aarninkhof, S. (2022). Subaqueous and subaerial beach changes after implementation of a mega nourishment in front of a sea dike. *Journal of Marine Science and Engineering*, *10*(8), 1152. https://doi.org/10.3390/JMSE10081152

Krumbein, W. C. (1934). Size frequency distributions of sediments. *Journal of Sedimentary Research*, *4*(2), 65–77. https://doi.org/10.1306/D4268EB9-2B26-11D7-8648000102C1865D

Liu, Y., Liu, X., & Sun, Y. (2021). QGrain: An open-source and easy-to-use software for the comprehensive analysis of grain size distributions. *Sedimentary Geology*, *423*, 105980. https://doi.org/10.1016/J.SEDGEO.2021.105980

McKenna Neuman, C., & Bédard, O. (2017). A wind tunnel investigation of particle segregation, ripple formation and armouring within sand beds of systematically varied texture. *Earth Surface Processes and Landforms*, *42*(5), 749–762. https://doi.org/10.1002/ESP.4019

McKenna Neuman, C., Li, B., & Nash, D. (2012). Micro-topographic analysis of shell pavements formed by aeolian transport in a wind tunnel simulation. *Journal of Geophysical Research*, *117*(F4), 4003. https://doi.org/10.1029/2012JF002381

Moayeri, V., Miri, A., Shahriari, A., Rahdari, V., & Gill, T. E. (2023). A field study of the surface disturbance effects of animals and motor vehicles on aeolian sediment emission from a silty playa surface. *Environmental Research*, *216*, 114606. https://doi.org/10.1016/J.ENVRES.2022.114606

Owen, P. R. (1964). Saltation of uniform grains in air. *Journal of Fluid Mechanics*, *20*(2), 225–242. https://doi.org/10.1017/S0022112064001173

Prodger, S., Russell, P., & Davidson, M. (2017). Grain-size distributions on high-energy sandy beaches and their relation to wave dissipation. *Sedimentology*, *64*(5), 1289–1302. https://doi.org/10.1111/sed.12353

Reniers, A. J. H. M., Gallagher, E. L., MacMahan, J. H., Brown, J. A., van Rooijen, A. A., van de Thiel Vries, J. S. M., & van Prooijen, B. C. (2013). Observations and modeling of steep-beach grain-size variability. *Journal of Geophysical Research: Oceans*, *118*(2), 577–591. https://doi.org/10.1029/2012JC008073

Reyes-Martínez, M. J., Ruíz-Delgado, M. C., Sánchez-Moyano, J. E., & García-García, F. J. (2015). Response of intertidal sandy-beach macrofauna to human trampling: An urban vs. natural beach system approach. *Marine Environmental Research*, *103*, 36–45. https://doi.org/10.1016/J.MARENVRES.2014.11.005

Roelvink, D., & Costas, S. (2019). Coupling nearshore and aeolian processes: XBeach and duna process-based models. *Environmental Modelling & Software*, *115*, 98–112. https://doi.org/10.1016/j.envsoft.2019.02.010

Sarre, R. D. (1987). Aeolian sand transport. *Progress in Physical Geography*, *11*(2), 157–182. https://doi.org/10.1177/030913338701100201/ASSET/030913338701100201.FP.PNG_V03

Sherman, D. J. (1992). An equilibrium relationship for shear velocity and apparent roughness length in aeolian saltation. *Geomorphology*, *5*(3–5), 419–431. https://doi.org/10.1016/0169-555x(92)90016-h

Sherman, D. J., & Farrell, E. J. (2008). Aerodynamic roughness lengths over movable beds: Comparison of wind tunnel and field data. *Journal of Geophysical Research*, *113*(F2), 2–08. https://doi.org/10.1029/2007JF000784

Sherman, D. J., Zhang, P., Martin, R. L., Ellis, J. T., Kok, J. F., Farrell, E. J., & Li, B. (2019). Aeolian ripple migration and associated creep transport rates. https://doi.org/10.3390/geosciences9090389

Sonu, C. J. (1972). Bimodal composition and cyclic characteristics of beach sediment in continuously changing profiles. *SEPM Journal of Sedimentary Research*, *42*(4), 852–857. https://doi.org/10.1306/74d72653-2b21-11d7-8648000102c1865d

Srisuwan, C., & Work, P. A. (2015). Beach profile model with size-selective sediment transport. II: Numerical modeling. *Journal of Waterway, Port, Coastal, and Ocean Engineering*, *141*(2), 04014033. https://doi.org/10.1061/(ASCE)WW.1943-5460.0000274

Stauble, D. K., & Cialone, M. A. (1997). Sediment dynamics and profile interactions: DUCK94. In *Proceedings of the coastal engineering conference* (Vol. 4, pp. 3921–3934). https://doi.org/10.1061/9780784402429.303

Swann, C., Lee, D., Trimble, S., & Key, C. (2021). Aeolian sand transport over a wet, sandy beach. *Aeolian Research*, *51*, 100712. https://doi.org/10.1016/J.AEOLIA.2021.100712

Uphues, C. F. K., van IJzendoorn, C. O., Hallin, C., Pearson, S. G., Prooijen, B. C., van da Silva, G. M., & de Vries, S. (2022). Coastal aeolian sediment transport in an active bed surface layer: Tracer study and conceptual model. *Earth Surface Processes and Landforms*, *47*(13), 3147–3162. https://doi.org/10.1002/ESP.5449

van der Wal, D. (2000a). Grain-size-selective aeolian sand transport on a nourished beach. *Journal of Coastal Research*, *16*(3).

van der Wal, D. (2000b). Modelling aeolian sand transport and morphological development in two beach nourishment areas. *Earth Surface Processes and Landforms*, *25*(1), 77–92. https://doi.org/10.1002/(SICI)1096-9837(200001)25:1<77::AID-ESP49>3.0.CO;2-M

Van Dijk, P. M., Arens, S. M., & Van Boxel, J. H. (1999). Aeolian processes across transverse dunes. II: Modelling the sediment transport and profile development. *Earth Surface Processes and Landforms*, *24*(4), 319–333. https://doi.org/10.1002/(sici)1096-9837(199904)24:4<319::aid-esp963>3.0.co;2-m

van IJzendoorn, C. O. (2023). Python code for the analysis of AeoLiS grain size scenarios (Version 1.1.0) [Software]. 4TU Repository. https://doi.org/10.4121/22220134

van IJzendoorn, C. O., Hallin, C., Cohn, N., Reniers, A. J. H. M., & de Vries, S. (2022). Novel sediment sampling method provides new insights into vertical grain size variability due to marine and aeolian beach processes. *Earth Surface Processes and Landforms*. https://doi.org/10.1002/ESP.5518

van Rijn, L. C., & Strypsteen, G. (2020). A fully predictive model for aeolian sand transport. *Coastal Engineering*, *156*, 103600. https://doi.org/10.1016/J.COASTALENG.2019.103600

Zhang, P., Sherman, D. J., & Li, B. (2021). Aeolian creep transport: A review. *Aeolian Research*, *51*, 100711. https://doi.org/10.1016/J.AEOLIA.2021.100711